Coating of $BaCO_3$ Crystals with TiO_2: Versatile Approach to the Synthesis of $BaTiO_3$ Tetragonal Nanoparticles

Maria Teresa Buscaglia,[†] Vincenzo Buscaglia,*[,†] and Rocco Alessio[‡]

Institute for Energetics and Interphases, National Research Council, via De Marini 6, I-16149 Genoa, Italy, and Solvay Bario e Derivati, Via degli Oliveti 84, I-54100 Massa, Italy

Received August 2, 2006. Revised Manuscript Received December 6, 2006

The fabrication of the very thin (<1 μm) dielectric layers for the next generation of miniaturized multilayer ceramic capacitors will require barium titanate, $BaTiO_3$, particles of 100−200 nm with narrow particle size distributions, high density, and high tetragonality. Composite particles, consisting of a $BaCO_3$ core and a TiO_2 shell, can be efficiently used for the solid-state synthesis of nanocrystalline tetragonal $BaTiO_3$ powders at moderate temperatures. A uniform layer of amorphous titania has been formed on the surface of fine barium carbonate crystals suspended in a peroxotitanium(IV) solution by a precipitation process. Formation of single phase $BaTiO_3$ from the $BaCO_3$@TiO_2 particles occurs by a single step reaction at 600−650 °C, whereas the conversion of mechanical mixtures of nanocrystalline raw materials $BaCO_3$ and TiO_2 requires temperatures ≥800 °C and produces much coarser powders. The lowering of the reaction temperature can be attributed to the maximization of the contact surface between the reactants and to the minimization of diffusion distances. The $BaCO_3$@TiO_2 particles undergo spontaneous fragmentation and spheroidization during the reaction, and, consequently, the resulting $BaTiO_3$ nanoparticles have no memory of the initial shape of the barium carbonate crystals. The final powders have high density (94−98%), high tetragonality (*c*/*a* ratio: 1.006), average particle size of 140 nm, and no agglomerates bigger than 300 nm. The solid-state reaction of $BaCO_3$@TiO_2 particles is a simple process that could be competitive with the oxalate and the hydrothermal routes for the mass production of high-quality $BaTiO_3$ nanopowders.

Introduction

Barium titanate is the ceramic material most widely used in the electronic industry (yearly production: ∼11 000 tons). With its high dielectric constant and low losses, it is an excellent dielectric material. The main application is the production of multilayer ceramic capacitors (MLCCs), the most common type of passive component in consumer electronics.[1] MLCCs have continued to evolve in two primary directions: smaller size (miniaturization) and larger capacitance values. In the very near future, the number of layers in a single capacitor will exceed 1000, while the thickness of the single ceramic layer will become <1 μm.[2] Considering that the thickness of a single dielectric layer should be comprised, as empirical rule, of about 5 grains, it is evident that the fabrication of these very thin layers requires well-dispersed, small, and uniform particles with a size of 100−200 nm. Fine powders of this kind are usually obtained by hydrothermal synthesis.[3] However, the MLCC market is nowadays very competitive, and the passive components companies are looking for less expensive alternatives to the hydrothermal powders, such as the solid-state route. Very small crystalline particles with diameter of the order of 10 nm were prepared by reaction of metal alkoxides dissolved in organic solvents or by microemulsion-mediated synthesis.[4,5] However, the cost of these powders is, at present, prohibitively high.

The nanoscale coating of small particles with a different compound is an effective tool to engineer their surface and functional properties. In particular, the synthesis of core−shell particles is attracting a great deal of interest because of the diverse applicability of these colloidal particles.[6,7] Typical examples include the modification of the surface properties by a silica coating to obtain particles that can be dispersed in a liquid medium or in a glass matrix,[8−10] the retardation of the sintering of metallic particles by oxide

* Corresponding author. Tel.: +39-010-6475708. Fax: +39-010-6475700. E-mail: v.buscaglia@ge.ieni.cnr.it.
† Institute for Energetics and Interphases.
‡ Solvay Bario e Derivati.

(1) Rae, A.; Chu, M.; Ganine, V. Barium titanate − Past, present and future. In *Dielectric Ceramic Materials*; Nair, K. M., Bhalla, A. S., Eds.; Ceramic Transactions Vol. 100; The American Ceramic Society: Westerville, OH, 1999; pp 1−12.
(2) (a) Reynolds, T. G., III. *Am. Ceram. Soc. Bull.* **2001**, *80*, 29. (b) Randall, C. A. *J. Ceram. Soc. Jpn.* **2001**, *109*, S2.
(3) Pithan, C.; Hennings, D.; Waser, R. *Int. J. Appl. Ceram. Technol.* **2005**, *2*, 1.
(4) (a) Beck, Ch.; Härtl, W.; Hempelmann, R. *J. Mater. Res.* **1998**, *13*, 3174. (b) Pithan, C.; Shiratori, Y.; Waser, R.; Dornseiffer, J.; Haegel, F.-H. *J. Am. Ceram. Soc.* **2006**, *89*, 2908.
(5) (a) O'Brien, S.; Brus, L.; Murray, C. B. *J. Am. Chem. Soc.* **2001**, *123*, 12085. (b) Niederberger, M.; Pinna, N.; Polleux, J.; Antonietti, M. *Angew. Chem., Int. Ed.* **2004**, *43*, 2270. (c) Niederberger, M.; Garnweitner, G.; Pinna, N.; Antonietti, M. *J. Am. Chem. Soc.* **2004**, *126*, 9120.
(6) Caruso, R. A.; Antonietti, M. *Chem. Mater.* **2001**, *13*, 3272.
(7) Caruso, F. *Adv. Mater.* **2001**, *13*, 11.
(8) Philipse, A. P.; van Bruggen, M. P. B.; Pathmamanoharan, C. *Langmuir* **1994**, *10*, 92.
(9) Liz-Marzan, L. M.; Giersig, M.; Mulvaney, P. *Langmuir* **1996**, *12*, 4329.
(10) (a) Ohmori, M.; Matijevic, E. *J. Colloid Interface Sci* **1993**, *160*, 288. (b) Hardikar, V. V.; Matijevic, E. *J. Colloid Interface Sci.* **2000**, *221*, 133.

10.1021/cm061823b CCC: $37.00
Published on Web 01/19/2007

coating,[11] the preparation of particles with tailored magnetic,[8,12] optical,[13−15] and catalytic[16,17] properties, the fabrication of hollow spheres,[18−20] and the realization of capsules for drug delivery.[21]

A further application of core−shell particles, which is the subject of this work, is the exploitation of the intimate contact between the core and the shell materials to facilitate the synthesis of ternary and even more complex solid compounds by solid-state reaction. Provided that the shell is uniform and continuous, the contact area between the reactants is maximized in a core−shell structure, and this should result in a significant decrease of the temperature required for the reaction. The lower is the temperature, the less important are the parasitic coarsening and sintering processes, which are well known to strongly affect the particle size and the particle size distribution of the final powders. In particular, the premature sintering and coalescence of nanosized particles at temperatures lower than or comparable to that of the solid-state reaction often jeopardize the potential advantages of using a nanocrystalline powder as a raw material. Thus, the shell can have a two-fold role: it acts as a reactant but also inhibits undesired sintering and coarsening.

In this study, the previous concepts have been applied to the solid-state synthesis of barium titanate, $BaTiO_3$. We describe the coating of $BaCO_3$ crystals with a layer of TiO_2 and the transformation of these $BaCO_3$@TiO_2 core−shell particles (Liz-Marzán et al.[9] introduced the A@B notation to signify A cores coated with a B shell) in single phase nanocrystalline $BaTiO_3$. The coating was obtained by the direct precipitation of the shell material at the surface of the cores suspended in a Ti(IV) solution. This technique is particularly suitable for the deposition of metal oxide coatings avoiding the use of organic solvents.[6,7] The coating process makes use of $TiCl_4$ as titanium source and results in uniform and continuous coatings. Moreover, it provides the possibility to carefully control the thickness of the TiO_2 layer. The methodology is completely different from the coating of TiO_2 particles with $BaCO_3$ described by Rössel et al.[22] In that work, TiO_2 particles were first coated with $Ba(OH)_2$ by means of spray drying, and then the hydroxide layer was carbonated to $BaCO_3$ by reaction with a CO_2 stream.

Barium carbonate is soluble in water at pH < 7. Thus, a certain difficulty is represented by the necessity to stabilize tetravalent titanium in an aqueous solution at a neutral or moderately alkaline pH (7−10). Highly acidic solutions of $TiCl_4$ are necessary to prevent hydrolysis and spontaneous precipitation of amorphous or crystalline TiO_2.[23] Stability at pH > 1 can be attained by complexation with suitable molecules. Rather stable Ti(IV) solutions in water can be obtained by using organic chelating agents, such as acetylacetone[24] and lactic acid. In particular, titanium(IV) bis(ammonium lactato) dihydroxide (TALH) is widely used for the preparation of thin films of TiO_2[25] or to coat different kinds of particles.[16,17] Hydrolysis of Ti(IV) solutions at pH < 3 can be suppressed by addition of hydrogen peroxide (H_2O_2) and formation of the peroxotitanium complex (TiO_2^{2+}) and other complexes, such as the dinuclear $Ti_2O_5^{2+}$ and the corresponding species generated by the deprotonation of coordinated water.[26,27] The stability of Ti(IV) aqueous solutions can be extended up to neutrality or even to pH 10 by using H_2O_2 together with a second chelating agent, such as molecules like EDTA or nitrilo triacetic acid.[27,28] Evidence that relatively stable Ti(IV) solutions with pH ≥7 can be obtained by addition of H_2O_2 and NH_3 was given by Gherardi and Matjievic[29] and, more recently, by Ichinose et al.,[30] Camargo and Kakihana,[31] and Gao et al.[32] After some preliminary experiments, the combination H_2O_2/NH_3 was selected for the preparation of the Ti(IV) solution for the coating of the carbonate. As a result, $BaCO_3$@TiO_2 core−shell particles could be obtained making use of inorganic precursors only. Furthermore, the process does not introduce foreign ions, which may be incorporated in the titanium oxide shell (residual ammonium and chloride ions, if any, are easily eliminated as NH_4Cl during the calcination step because this salt sublimes at 340 °C).

As the size of the particles is not the unique parameter to define the applicability of a $BaTiO_3$ powder for production of ceramic capacitors, we have carried out a careful characterization of the final product obtained by calcination of the coated powder. A further objective of this study is to show that the enhanced reactivity of the $BaCO_3$@TiO_2 particles is not uniquely related to the nanocrystalline nature

(11) Lee, J.-Y.; Lee, J.-H.; Hong, S.-H.; Lee, Y. K.; Choi, J.-Y. *Adv. Mater.* **2003**, *15*, 1655.
(12) Aliev, F. G.; Correa-Duarte, M. A.; Mamedov, A.; Ostrander, J. W.; Giersig, M.; Liz-Marzan, L. M.; Kotov, N. A. *Adv. Mater.* **1999**, *11*, 1006.
(13) (a) Oldenburg, S. J.; Averitt, R. D.; Westcott, S. L.; Halas, N. J. *Chem. Phys. Lett.* **1998**, *288*, 243. (b) Oldenburg, S. J.; Jackson, J. B.; Westcott, S. L.; Halas, N. J. *Appl. Phys. Lett.* **1999**, *75*, 2897.
(14) Mulvaney, P.; Liz-Marzan, L. M.; Giersig, M.; Ung, T. *J. Mater. Chem.* **2000**, *10*, 1259.
(15) (a) Cassagneau, T.; Caruso, F. *Adv. Mater.* **2002**, *14*, 732. (b) Salgueirino-Maceira, V.; Caruso, F.; Liz-Marzan, L. M. *J. Phys. Chem. B* **2003**, *107*, 10990. (c) Schuetz, P.; Caruso, F. *Chem. Mater.* **2002**, *14*, 4509.
(16) Subramanya Mayya, K.; Gittings, D. I.; Caruso, F. *Chem. Mater.* **2001**, *13*, 3833.
(17) Lee, S.-w.; Drwiega, J.; Wu, C.-Y.; Mazyck, D.; Sigmund, W. M. *Chem. Mater.* **2004**, *16*, 1160.
(18) Kawahashi, N.; Persson, C.; Matijevic, E. *J. Mater. Chem.* **1991**, *1*, 577.
(19) Walsh, D.; Mann, S. *Nature* **1995**, *377*, 320.
(20) (a) Caruso, F.; Caruso, R. A.; Möhwald, H. *Science* **1998**, *282*, 1111. (b) Caruso, F.; Shi, X.; Caruso, R. A.; Susha, A. *Adv. Mater.* **2001**, *13*, 740.
(21) (a) Radt, A.; Smith, T. A.; Caruso, F. *Adv. Mater.* **2004**, *16*, 2184. (b) Khopade, A. J.; Caruso, F. *Chem. Mater.* **2004**, *16*, 2107.
(22) Rössel, M.; Gablenz, S.; Müller, T.; Röder, A.; Abicht, H.-P. *Anal. Bioanal. Chem.* **2003**, *375*, 310.
(23) (a) Kim, S.-J.; Park, S.-D.; Jeong, Y.-H.; Park, S. *J. Am. Ceram. Soc.* **1999**, *82*, 927. (b) Zhang, Q.; Gao, L.; Guo, J. *J. Eur. Ceram. Soc.* **2000**, *20*, 2153.
(24) (a) Leaustic, A.; Babonneau, F.; Livage, J. *Chem. Mater.* **1989**, *1*, 240. (b) Leaustic, A.; Babonneau, F.; Livage, J. *Chem. Mater.* **1989**, *1*, 248.
(25) Shi, X.; Cassagneau, T.; Caruso, F. *Langmuir* **2002**, *18*, 904.
(26) (a) Gastinger, E. *Z. Anorg. Allg. Chem.* **1954**, *275*, 331. (b) Rotzinger, F. P.; Grätzel, M. *Inorg. Chem.* **1987**, *26*, 3704. (c) Fox, G. R.; Adair, J. H.; Newnham, R. E. *J. Mater. Sci.* **1990**, *25*, 3634.
(27) Mühlebach, J.; Müller, K.; Schwarzenbach, G. *Inorg. Chem.* **1970**, *9*, 2381.
(28) Wada, S.; Chikamori, H.; Noma, T.; Suzuki, T. *J. Mater. Sci. Lett.* **2000**, *19*, 1855.
(29) Gherardi, P.; Matijevic, E. *Colloids Surf.* **1988**, *32*, 257.
(30) Ichinose, H.; Terasaki, M.; Katsuki, H. *J. Sol.-Gel Sci. Technol.* **2001**, *22*, 33.
(31) Camargo, E. M.; Kakihana, M. *Chem. Mater.* **2001**, *13*, 1181.
(32) Gao, Y. F.; Masuda, Y.; Peng, Z. F.; Yonezawa, T.; Koumoto, K. *J. Mater. Chem.* **2003**, *13*, 608.

of the carbonate. Therefore, we have compared the results to the properties of a very fine powder obtained by the conventional solid-state process starting from nanocrystalline raw materials.

Experimental Section

Materials. Electronic-grade purity nanocrystalline barium carbonate (BC, witherite phase, $S_{BET} = 31\ m^2\ g^{-1}$, $d_{BET} = 48$ nm, $d_{v50} = 116$ nm) was provided by Solvay Bario e Derivati (Massa, Italy). The powder consists of elongated crystals with length of 100−500 nm and aspect ratio of 2−10 (see the Supporting Information, Figure S1). $TiCl_4$ (99.9%) was obtained from Acros Chemicals. Ammonia (6 M) and H_2O_2 (30 vol %) solutions in water were obtained from Aldrich. The water used in all experiments was freshly distilled.

Preparation of the Ti(IV) Solution. A $TiOCl_2$ mother solution (2.8 mol kg^{-1}) was prepared by drop-by-drop addition of $TiCl_4$ in water cooled in a ice bath. In a typical experiment, the required amount of the mother solution was diluted with water to obtain 300 dm^3 of a Ti(IV) solution with concentration of 0.13 mol dm^{-3}. During the next preparation steps, the solution was kept at a temperature below 5 °C by an ice bath. The H_2O_2 solution (21 dm^3) was slowly added to the Ti(IV) solution while stirring. The final clear solution showed a dark orange color, indicative of the formation of the peroxotitanium complex. The ammonia solution was slowly added to the solution of the peroxocompound under vigorous stirring until the pH attained a value of ∼9. During the addition, the color of the solution progressively turned light yellow. The final solution was stable for a few days if kept at a temperature of 5−10 °C. For longer times, the solution became opaque, and formation of a yellow precipitate was observed.

Coating of the $BaCO_3$ Cores. The BC powder was suspended in the Ti(IV) solution (prepared as described above) at room temperature while stirring. The amount of carbonate was that required to obtain a given Ba/Ti molar ratio (usually 1) in the suspension. Because there was not appreciable loss of either barium or titanium during the coating process, the final coated powder had the same overall Ba/Ti stoichiometry of the suspension. The suspension was slowly heated to 95 °C and kept at this temperature for 5 h. The solid phase, a white powder, was then separated from the liquid by filtration, washed until chloride ions were no longer detected in the supernatant (test with a 0.1 M silver nitrate solution, detection limit of the order of ppm), and finally dried.

Characterization of the $BaCO_3$@TiO_2 Core−Shell Particles and Reactivity. Particle morphology and composition of the as-prepared powder as well as of the powder after calcination at different temperatures in the range 500−700 °C were studied by different techniques. The phase composition was investigated by means of X-ray diffraction (XRD, Philips PW1710, Co Kα radiation) and Raman spectroscopy. The Raman spectra were collected using a He−Ne laser (633 nm) on the surface of pressed pellets by a micro-Raman spectrometer (Renishaw, Wolton-under-Edge, UK) in the wavenumber range 200−1200 cm^{-1}. The characteristic bands of Ti-peroxy gels, TiO_2 polymorphs, $BaCO_3$, and $BaTiO_3$ are located in this spectral region. Scanning electron microscopy (SEM) observations were conducted with a LEO 1450VP instrument operated at 15 kV. High-resolution transmission electron microscopy (HRTEM) and electron diffraction were performed with a JEOL 2010 microscope operated at 200 kV and equipped with an energy dispersive X-ray analyzer. The reaction between the $BaCO_3$ core and the TiO_2 shell was studied by means of thermogravimetric analysis (TG) and differential thermal analysis (DTA), performed at a heating rate of 5 °C min^{-1} in 0.1 L min^{-1} flow of dry air at ambient pressure.

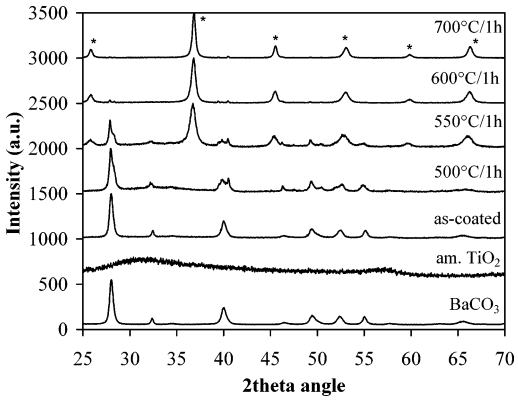

Figure 1. XRD (Co Kα radiation) patterns of (from the bottom): $BaCO_3$ starting powder, amorphous titania obtained by hydrolysis of the Ti(IV) precursor solution, $BaCO_3$ particles coated with amorphous titania, and $BaCO_3$@TiO_2 particles calcined for 1 h at different temperatures between 500 and 700 °C. The asterisks indicate the peaks of $BaTiO_3$.

Calcination and Characterization of $BaTiO_3$ Powders. The as-prepared coated powders were fired in air in a muffle furnace at different temperatures between 650 and 1000 °C. The heating rate was 5 °C/min, and the duration of the isothermal treatment was either 2 or 4 h. The lattice parameters of $BaTiO_3$ were obtained by Rietveld refinement of the XRD patterns collected with a scan step of 0.025° 2θ and a sampling time of 10 s. The crystallite size was estimated by means of the Scherrer equation from the broadening of the 111 peak after correction for instrumental broadening by a silicon standard. The density, ρ, of the powders was measured by helium picnometry (Micromeritics Accupyc 1330). The specific surface area, S_{BET}, was measured by nitrogen adsorption (Micromeritics ASAP 2010) according to the BET method. The equivalent BET diameter, d_{BET}, was calculated as $d_{BET} = 6/\rho S_{BET}$. Particle size distributions (PSD) were measured by means of an X-ray disc photocentrifuge (Bi-XDC, Brokhaven Instruments Corp., Holtsville, NY) and are presented as volume-based distributions. The span of the PSD was defined as $(d_{v90} - d_{v10})/d_{v50}$, where d_{vp} is the diameter corresponding to the % p of particles with size less than this diameter in the cumulative particle size distribution.

Preparation of a Reference Sample. To compare the reactivity of the $BaCO_3$@TiO_2 particles as well as the properties of the final $BaTiO_3$ powders with the conventional solid-state process, a mixture of the same BC powder used for the coating process and of a nanocrystalline TiO_2 (Toho Titanium, Chigasaki, Japan, grade HT2301, $S_{BET} = 22.5\ m^2\ g^{-1}$, $d_{BET} = 67$ nm, $d_{v50} = 170$ nm) was prepared by ball milling in water, as described in detail elsewhere.[33] This mixture, denoted as BTSS, was subjected to the same thermal treatments of the coated powder.

Results and Discussion

Morphology and Composition of the $BaCO_3$@TiO_2 Core−Shell Particles. The XRD pattern of the as-coated and dried powder (Figure 1) shows only the peaks of witherite $BaCO_3$, meaning that the coating is mainly composed of an amorphous phase. A detailed observation reveals, superimposed on the diffraction pattern of $BaCO_3$, a broad hump of weak intensity at 25−40° 2θ (not visible in Figure 1), which can be ascribed to the amorphous coating. Hydrolysis of the Ti(IV) solution in the same experimental conditions but in the absence of suspended $BaCO_3$ produces

(33) Buscaglia, M. T.; Bassoli, M.; Buscaglia, V.; Alessio, R. *J. Am. Ceram. Soc.* **2005**, *88*, 2374.

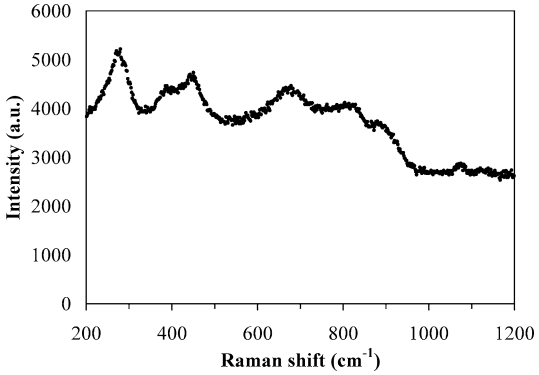

Figure 2. Raman spectrum of the precipitate obtained by hydrolysis of the peroxo-Ti(IV) solution at 95 °C.

a pale yellow amorphous precipitate, which shows the typical diffraction pattern of amorphous titania,[34,35] with two broad humps centered at ~32° 2θ and ~57° 2θ (Figure 1). The maximum diffraction intensity of this amorphous titania is about 20 times lower that that of $BaCO_3$, making this phase hardly detectable by ordinary XRD when mixed with the carbonate. According to the available literature,[27,36−38] hydrolysis of peroxotitanium solutions at room temperature produces an amorphous phase of peroxotitanium hydrate with not yet well-known structure. However, the peroxotitanium hydrate decomposes rapidly to amorphous (hydrated) titania (AT) at temperatures of the order of 80−100 °C.[36−38] Therefore, it is likely that the amorphous coating obtained in the present study is mainly composed by AT containing hydration water. This is confirmed by the results of the Raman investigation. The precipitate obtained by hydrolysis of the Ti(IV) solution in the absence of $BaCO_3$ shows several broad features located at 280, 390, 455, 680, 825, 890, and 1080 cm^{-1} (Figure 2). However, only the features at 280, 455, and 680 cm^{-1} can be considered as well-defined peaks. The above bands have frequencies close to the vibration modes (285, 395, 480, 650, 800, 910−930 cm^{-1}) of the Ti−O−Ti groups in titanium-containing dimers and oligomers,[37,39] although a band at 350 cm^{-1} (not observed) is also expected. The distinctive feature of the Ti−O−O groups in peroxy titanium gels,[37] a strong band at 525 cm^{-1}, is not observed, thus excluding the presence of a significant amount of residual peroxy groups. The Raman spectra of amorphous titania precipitated by neutralizing $TiCl_4$ solution with sodium carbonate up to pH 9[34] or aqueous NH_3 up to pH 11[40] show broad bands at 275−280, 385−390, and 445−450 cm^{-1}, in agreement with Figure 1. Peaks at 285, 380, 440, 620, and 680 cm^{-1} were observed in partially transformed Ti-peroxy gels after 6 months aging in the aqueous state.[37]

The coating process results in $BaCO_3$@TiO_2 particles with a continuous and uniform AT layer, as shown in Figure 3. The coating is composed of amorphous particles of 5−10 nm. Electron diffraction and observation in high resolution give no evidence of crystalline TiO_2. The formation of the coating is attributed to the different sign of the surface potential of the two solid phases at the pH used for the synthesis. The zeta potential of $BaCO_3$ becomes negative at pH > 10,[41] while this already happens at pH > 6 for TiO_2.[42] Consequently, in the pH window 6−10, the zeta potential of $BaCO_3$ is positive, while that of TiO_2 is negative. Moreover, between pH 8 and 9, the absolute value of the zeta potential of the two solids is rather high (~40 mV). Therefore (assuming for AT a behavior similar to crystalline TiO_2), the AT clusters and nanoparticles produced by the hydrolysis of the Ti(IV) solution will have a spontaneous tendency to self-assemble at the surface of the $BaCO_3$ crystals.

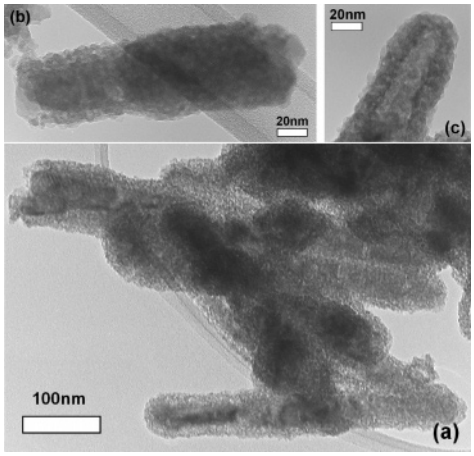

Figure 3. Morphology (TEM) of $BaCO_3$@TiO_2 crystals. (a) A group of coated particles. (b) An isolated coated nanocrystal. (c) A detail from a bundle of coated crystals.

Formation of $BaTiO_3$ by the Solid-State Reaction between the TiO_2 Shell and the $BaCO_3$ Core. According to the XRD patterns of powders heated for 1 h at different temperatures in the range 500−700 °C (Figure 1), formation of $BaTiO_3$ starts between 500 and 550 °C and is practically finished at 600 °C. The diffraction patterns collected at 550 and 600 °C clearly show the peaks of whiterite-$BaCO_3$ and pseudo-cubic $BaTiO_3$. Other phases (e.g., rutile, anatase, Ba_2TiO_4), if any, are below the XRD detection limit (of the order of 1−2 wt %). Therefore, it can be assumed that, above 500 °C, the AT shell reacts with the $BaCO_3$ core with formation of crystalline $BaTiO_3$ and gaseous CO_2.

The constant heating rate (5 °C min^{-1}) thermogravimetric curve of the coated powder (not shown) reveals a first weight loss between 40 and 200 °C, which can be ascribed to the evaporation of water from the AT coating, and a second weight loss between 500 and 700 °C. The latter weight loss, according to the XRD results (Figure 1), is related to the formation of $BaTiO_3$. The temperatures at which the formation of $BaTiO_3$ takes place with the maximum rate can be better appreciated from the curve of the first derivative of the weight loss (see Figure 4), usually called differential thermal gravimetry (DTG). Only a single DTG peak at

(34) Yin, H.; Wada, Y.; Kitamura, T.; Kambe, S.; Murasawa, S.; Mori, H.; Sakata, T.; Yanagida, S. *J. Mater. Chem.* **2001**, *11*, 1694.
(35) Zhang, H.; Finnegan, M.; Banfield, J. F. *Nano Lett.* **2001**, *1*, 81.
(36) Tengvall, P.; Bertilsson, L.; Liedberg, B.; Elwing, H.; Lundstron, I. *J. Colloid Interface Sci.* **1990**, *139*, 575.
(37) Tengvall, P.; Vikinge, T. P.; Lundstron, I.; Liedberg, B. *J. Colloid Interface Sci.* **1993**, *160*, 10.
(38) Niesen, T. P.; Bill, J.; Aldinger, F. *Chem. Mater.* **2001**, *13*, 1552.
(39) Reichmann, M. G.; Bell, A. T. *Langmuir* **1987**, *3*, 111.
(40) Yanagisawa, K.; Ovenstone, J. *J. Phys. Chem. B* **1999**, *103*, 7781.
(41) Li, C.-C.; Jean, J.-H. *J. Am. Ceram. Soc.* **2002**, *85*, 2977.
(42) (a) Bae, H. S.; Lee, M. K.; Kim, W. W.; Rhee, C. K. *Colloids Surf., A* **2003**, *220*, 169. (b) Shi, Y.; Wu, Y.; Li, G. *J. Dispersion Sci. Technol.* **2003**, *24*, 739.

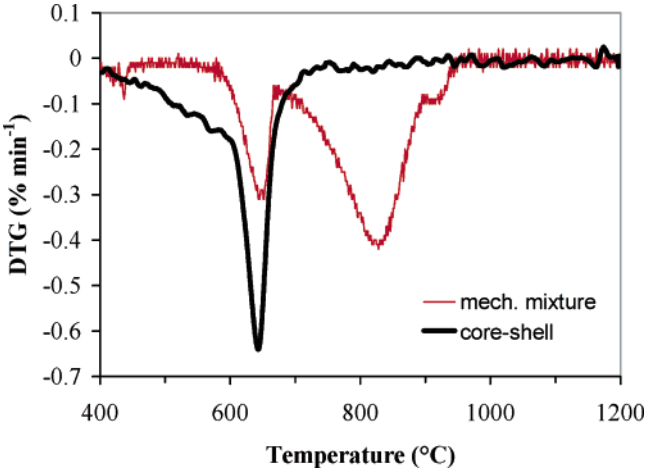

Figure 4. First derivative (DTG) of the weight loss curve from thermogravimetric analysis. Thick line: $BaCO_3$@TiO_2 particles. Thin line: mechanical mixure of nanocrystalline raw materials ($BaCO_3$ and TiO_2).

~650 °C is observed for the coated powder. The reaction starts around 500 °C, proceeds rapidly between 600 and 670 °C, and is nearly completed at ~750 °C. In agreement, the DTA curve (not reported) shows a single broad endothermic peak centered at ~630 °C. In contrast, the mechanical mixture of the nanocrystalline raw materials shows three distinct DTG peaks at ~650, ~830, and ~930 °C (faint), respectively. Thus, the complete formation of $BaTiO_3$ from the $BaCO_3$@TiO_2 particles at constant heating rate occurs by a single reaction stage at temperatures that are ~200 °C lower than those required for the mechanical mixture of the nanocrystalline oxides (same heating rate). This conclusion is also supported by recent results on the synthesis of ultrafine $BaTiO_3$ powders from homogeneous mixtures of nanocrystalline precursors $BaCO_3$ and TiO_2.[43] In these cases, the reaction of mechanical mixtures involves at least two different steps, and formation of a single phase product requires temperatures of the order of 800 °C.

The improvement is even more impressive if we consider that the solid-state reaction from conventional micrometer-sized raw materials requires a temperature of 1000−1100 °C. Taking into account that the thermodynamic decomposition temperature of $BaCO_3$ in air is ~820 °C,[33] it follows that the formation of $BaTiO_3$ from the $BaCO_3$@TiO_2 particles directly involves solid $BaCO_3$ according to the solid-state reaction:

$$BaCO_3(c) + TiO_2(a,c) \rightarrow BaTiO_3(c) + CO_2(g) \qquad (1)$$

without the preliminary decomposition in BaO and CO_2. Reaction 1 occurs between crystalline carbonate and titania, the latter either in amorphous or in nanocrystalline state, and produces nanocrystalline titanate and gaseous carbon dioxide. This interpretation is supported by the recent results reported by Lotnyk et al.[44] for diffusion couples obtained by evaporating a thin $BaCO_3$ film on TiO_2 single crystals. Formation of $BaTiO_3$ was observed at temperatures ≥625 °C, in agreement with our results. The Gibbs free energy variation of reaction 1 in air ($p(CO_2) = 3 \times 10^{-4}$ atm), calculated from the available thermochemical data[45] of the thermodynamically stable phases (rutile, whiterite, tetragonal $BaTiO_3$), turns out to be quite negative, −93 kJ mol^{-1} at 600 °C and −138 kJ mol^{-1} at 800 °C. Consequently, reaction 1 is strongly favored from the thermodynamic point of view. A DTG peak at ~650 °C was also observed on the DTG curve of the mechanical mixture (Figure 4). However, the contact area between the two reactants in the mechanical mixture is much smaller than that in the core−shell particles, and, consequently, most reaction occurs around or above the $BaCO_3$ decomposition temperature and probably involves BaO as an intermediate active species.[33]

Therefore, the improved reactivity of the coated particles with respect to the mechanical mixture can be mainly ascribed to the fact that the contact area between the reactants is maximized by the core−shell geometry. Furthermore, this arrangement minimizes the diffusion distance. Because the formation of nanocrystalline $BaTiO_3$ by decomposition of barium titanyl oxalate requires a temperature of 600−650 °C,[46] the solid-state reaction of $BaCO_3$@TiO_2 particles can compete with the oxalate route largely used at the industrial level.

The change of the shape of the $BaCO_3$ peaks in the XRD pattern collected on the powder annealed at 500 °C (Figure 1) indicates that some internal recrystallization of the carbonate occurs before the perovskite formation. The broad hump between 25° and 40° 2θ can be attributed to the amorphous titania coating and to the presence of very small rutile/anatase nuclei and crystallites. TEM observation of the powder calcined at 500 °C (Figure 5) shows that the coated crystals have retained the original shape, although the coating layer appears to be thinner, smoother, and more compact than in the as-coated particles (Figure 1). This indicates the loss of hydration water and densification of the coating during the annealing process. The thickness of the coating is 10−20 nm. Small nanocrystals (5−10 nm) were detected inside the amorphous titania coating by TEM, and the corresponding ED patterns (Figure 5) are compatible with rutile (JCPDS 21-1276). The ED patterns show also faint and diffuse circles ascribed to amorphous titania. The major phase after 1 h calcination at 550 °C is already barium titanate (Figure 1). The morphology of the particles calcined at 550 °C (Figure 6) corresponds to a chaotic ensemble of fragments caused by the disintegration of the coated particles. Despite the fragmentation, it is apparent from the TEM image that the reaction has initially produced the transformation of the original titania coating in a empty barium titanate shell, whereas the $BaCO_3$ core has mostly disappeared. This is consistent with the general mechanism of the solid-state reaction between $BaCO_3$ and TiO_2. According to previous studies,[47−50] formation of a $BaTiO_3$ layer occurs at the $BaCO_3$/TiO_2 interface, and further growth proceeds by

(43) (a) Ando, C.; Yanagawa, R.; Chazono, H.; Kishi, H.; Senna, M. *J. Mater. Res.* **2004**, *19*, 3592. (b) Ando, C.; Kishi, H.; Oguchi, H.; Senna, M. *J. Am. Ceram. Soc.* **2006**, *89*, 1709.
(44) Lotnyk, A.; Senz, S.; Hesse, D. *Solid State Ionics* **2006**, *177*, 429.
(45) Knacke, O.; Kubaschewski, O.; Hesselmann, K. *Thermochemical Properties of Inorganic Substances*; Verlag: Berlin, 1991.
(46) (a) Polotai, A. V.; Ragulya, A. V.; Tomila, T. V.; Randall, C. A. *Ferroelectrics* **2004**, *298*, 243. (b) Caruntu, G.; Rarig, R., Jr.; Dumitru, I.; O'Connor, C. J. *J. Mater. Chem.* **2006**, *16*, 752. (c) Hoshina, T.; Kakemoto, H.; Tsurumi, T.; Wada, S.; Yashima, M. *J. Appl. Phys.* **2006**, *99*, 054311.

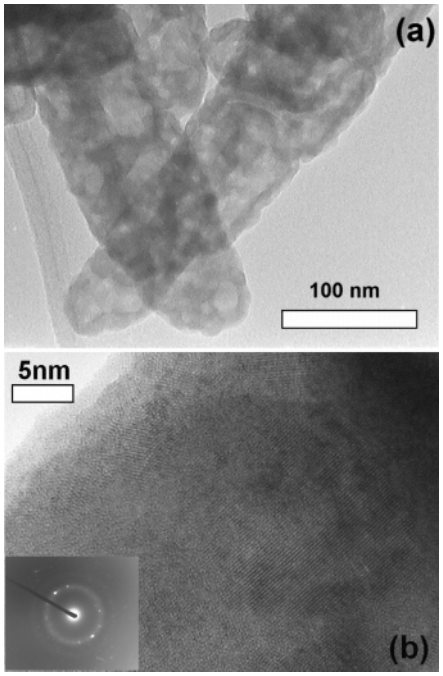

Figure 5. Morphology (TEM) of $BaCO_3$@TiO_2 particles after 1 h calcination at 500 °C. (a) General morphology. (b) Magnification of the amorphous TiO_2 coating showing a rutile nanocrystal. The inset shows the corresponding ED pattern.

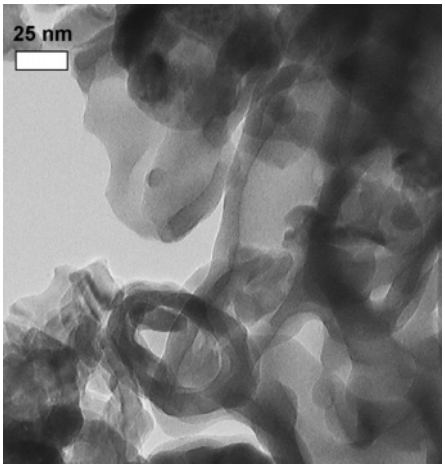

Figure 6. Morphology (TEM) of $BaCO_3$@TiO_2 particles after 1 h calcination at 550 °C.

diffusion of the barium ions across the perovskite layer toward the $BaTiO_3$/TiO_2 interface. However, we lack the detailed information on the initial stages of the reaction in the present system, including processes at the interfaces, nucleation of reaction products, and further growth. The fragmentation of the $BaTiO_3$/TiO_2 shells can have a two-fold origin. First, the internal CO_2 pressure generated by the solid-state reaction 1 inside the TiO_2 shell can be high enough to break the $BaTiO_3$/TiO_2 shell. Indeed, the titania layer appears to be rather compact and nonporous, making it

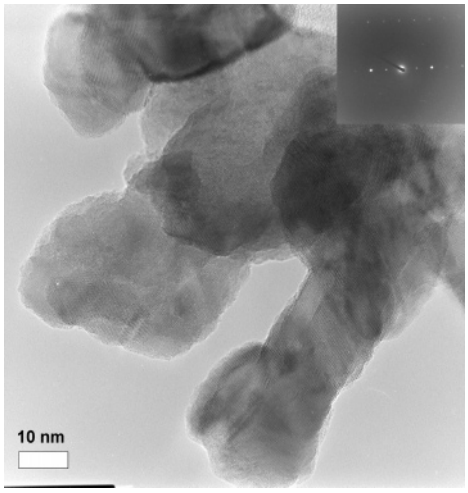

Figure 7. $BaTiO_3$ nanocrystals formed after 1 h calcination at 550 °C of $BaCO_3$@TiO_2 particles. The inset shows the ED pattern of a single nanoparticle.

difficult for the outward migration of CO_2 (Figures 5 and 6). Using the available thermochemical data,[45] it can be calculated that the equilibrium CO_2 pressure of reaction 1 at 550 °C attains the considerable value of 67 atm. Second, the volume increase accompanying the transformation of TiO_2 into $BaTiO_3$ (the ratio of the molar volumes is about 2) produces local stresses, which lead to the cracking of the $BaTiO_3$/TiO_2 layer. This process is facilitated by the absence of plastic deformation in TiO_2 at these temperatures and by the high radius of curvature of the surfaces. Although both fragmentation mechanisms are plausible, identification of the prevailing mechanism cannot be made on the basis of the available data. TEM observation shows that the fragments consist of a mixture of amorphous and nanocrystalline phases. Detailed examination of the fragments in which transformation is more advanced (Figure 7) reveals that they are composed of aggregates of crystallites of 10−20 nm, a size consistent with a crystallite diameter of 15 nm estimated from the XRD pattern by Scherrer equation. The ED pattern (see the inset of Figure 7 as an example) of these crystallites corresponds to $BaTiO_3$ (JCPDS 5-626). Powders calcined for 1 h at 700 °C are composed of essentially phase pure and crystalline $BaTiO_3$ with traces of $BaCO_3$ (Figure 1). TEM observation (Figure 8) shows primary nanograins in the range 25−50 nm, which form polycrystalline aggregates (secondary particles) with a diameter of 100−150 nm. The primary crystals inside the aggregates are sintered together, with the formation of grain boundaries (Figure 8). The lattice fringes are regular and parallel across each nanocrystal, indicating the absence of defects such as internal voids and surfaces, dislocations, twins, and stacking faults (see the Supporting Information, Figure S2). The absence of twins indicates that the $BaTiO_3$ nanograins are free of 90° ferroelectric domain walls. The crystallite size determined by the Scherrer equation from the XRD pattern is 34 nm. With increasing temperature (from 550 to 700 °C), the fragments of the shell undergo further fragmentation, spheroidization, and coarsening processes driven by the tendency to minimize the surface energy of the solid. Observation at lower magnification by SEM (see the Supporting Information, Figure S3) clearly shows that the final morphology of the $BaTiO_3$ particles

(47) Beauger, A.; Mutin, J. C.; Niepce, J. C. *J. Mater. Sci.* **1983**, *18*, 3041.
(48) Amin, A.; Spears, M. A.; Kulwicki, B. M. *J. Am. Ceram. Soc.* **1983**, *66*, 733.
(49) Rössel, M.; Höche, H.-R.; Leipner, H. S.; Völtzke, D.; Abicht, H.-P.; Hollricher, O.; Müller, J.; Gablenz, S. *Anal. Bioanal. Chem.* **2004**, *380*, 157.
(50) Graff, A.; Senz, S.; Voltzke, D.; Abicht, H.-P.; Hesse, D. *J. Eur. Ceram. Soc.* **2005**, *25*, 2201.

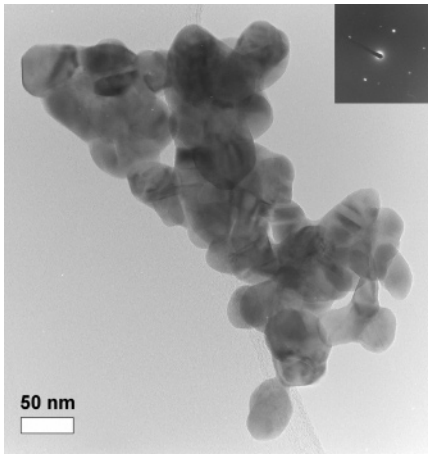

Figure 8. $BaTiO_3$ nanocrystals formed after 1 h calcination at 700 °C of $BaCO_3$@TiO_2 particles. The inset shows the ED pattern of a single nanoparticle.

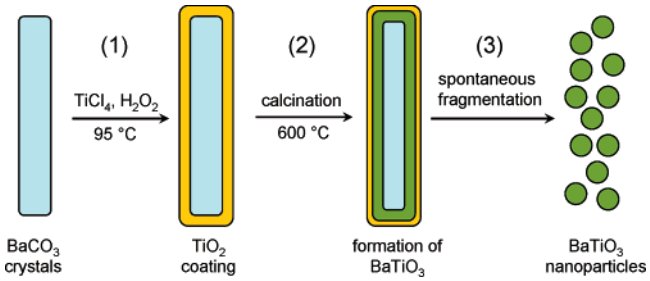

Figure 9. Schematic representation of the different processes leading to the formation of $BaTiO_3$ nanoparticles from $BaCO_3$ acicular crystals. Step 1 represents the coating of the $BaCO_3$ crystals suspended in a peroxotitanium(IV) solution with an amorphous TiO_2 layer by precipitation. Step 2 represents the formation of crystalline $BaTiO_3$ by reaction between the $BaCO_3$ core and the TiO_2 shell at ~600 °C. Step 3 corresponds to the spontaneous fragmentation of the shell in $BaTiO_3$ nanoparticles.

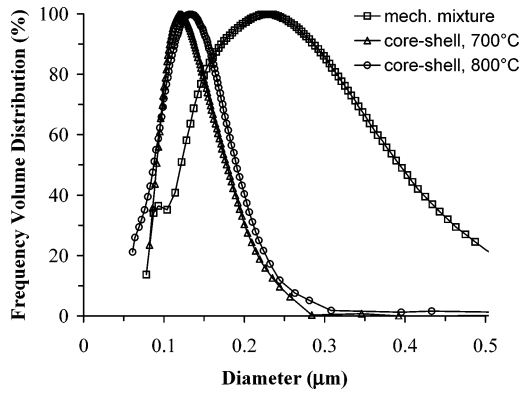

Figure 10. Particle size distribution (volume) of $BaTiO_3$ powders obtained by 2 h calcination of $BaCO_3$@TiO_2 particles at 700 and 800 °C. The PSD of a powder obtained by conventional solid-state reaction of a mechanical mixture of nanocrystalline raw materials ($BaCO_3$ and TiO_2) is reported for comparison.

resulting from the solid-state reaction has no memory of the original shape of the $BaCO_3$-coated crystals. The spheroidal particles of ~100 nm observed at SEM correspond to the polycrystalline aggregates revealed by TEM.

On the basis of the detailed XRD and TEM analyses, the different processes leading to the formation of $BaTiO_3$ nanoparticles from acicular $BaCO_3$ crystals have been schematically summarized in Figure 9. From a more general point of view, it is expected that core−shell structures obtained by means of colloidal chemistry can represent a new type of precursor for the mass production of high-quality, relatively cheap nanoparticles of different materials, providing similar mechanisms are involved.

Properties of the Final $BaTiO_3$ Powders. The properties of the phase pure $BaTiO_3$ powders obtained by calcination of the $BaCO_3$@TiO_2 particles at different temperatures (650−800 °C) are reported in Table 1. The small amounts of residual $BaCO_3$ detected after 1 h calcination (Figure 1) practically disappear after 4 h calcination at 650 °C or 2 h calcination at 700 °C. Accordingly, the XRD patterns of the final powders only show the peaks of $BaTiO_3$ (see the Supporting Information, Figure S4, as an example). Other phases (Ba_2TiO_4, polytitanates), if any, are below the detection limit (~1%) of XRD. This indicates that the powders are essentially stoichiometric. The XRD patterns (see the Supporting Information, Figure S4, as an example) correspond to the tetragonal structure with a c/a (c and a are the lattice parameters) ratio of 1.006 (from Rietveld profile fitting, $R_{wp} \approx 11\%$), to be compared to the reference value of 1.01 reported for single crystals and coarse ceramics. The characteristic splitting of the XRD peaks of tetragonal $BaTiO_3$ is hidden by the broadening effect related to the small crystallite size and the reduced tetragonality. Nevertheless, it is evident that the width of the 111 peak (at 45.5° 2θ), which is not subjected to splitting during the cubic to tetragonal transformation, is significantly smaller than that of the 200 peak (at 53° 2θ) and of the other surrounding peaks. The same considerations apply to the 222 peak (101.3° 2θ). At high 2θ angle, the peaks become slightly asymmetric (low angle side). In particular, it is evident that the pseudo cubic 311 reflection (~95.6° 2θ) consists of two tetragonal components, 113 and 311. Similar XRD patterns were recently reported by Pithan et al.[4] for tetragonal nanocrystalline $BaTiO_3$ particles obtained by microemulsion-mediated synthesis followed by calcination at different temperatures. Further evidence that the present powders correspond to the tetragonal modification of barium titanate is provided by the Raman spectrum (see the Supporting Information, Figure S5), which only shows well-defined bands at 270, 308, 523, and 720 cm^{-1}, characteristic of ferroelectric $BaTiO_3$.[51] The orthorhombic modification should show a peak or shoulder at about 487 cm^{-1}, which is not observed. However, coexistence of both the tetragonal and the orthorhombic ferroelectric modifications, as proposed in the case of nanocrystalline ceramics, cannot be completely excluded because of the similarity of the Raman scattering features of the two phases.[52] Despite the small crystallite size (24 nm after calcination at 650 °C and 52 nm after calcination at 800 °C), the present powders possess a high density (94−98% of the theoretical density, 6.01 g cm^{-3}) and a high tetragonality ($c/a = 1.006$). Many hydrothermal powders with comparable crystallite size described in the literature have

(51) (a) Perry, C. H.; Hall, D. B. *Phys. Rev. Lett.* **1965**, *15*, 700. (b) DiDomenico, M.; Wemple, S. H.; Porto, S. P. S. *Phys. Rev.* **1968**, *174*, 522. (c) Baskaran, N.; Ghule, A.; Bhongale, C.; Murugan, R.; Chang, H. *J. Appl. Phys.* **2002**, *91*, 10038.

(52) (a) Buscaglia, V.; Buscaglia, M. T.; Viviani, M.; Ostapchuk, T.; Gregora, I.; Petzelt, J.; Mitoseriu, L.; Nanni, P.; Testino, A.; Calderone, R.; Harnagea, C.; Zhao, Z.; Nygren, M. *J. Eur. Ceram. Soc.* **2005**, *25*, 3059. (b) Deng, X. Y.; Wang, X. H.; Wen, H.; Kang, A. G.; Gui, Z. L.; Li, L. T. *J. Am. Ceram. Soc.* **2006**, *89*, 1059.

Table 1. Properties of $BaTiO_3$ Powders Obtained by Calcination of $BaCO_3$@TiO_2 Particles at Different Temperatures

temperature (°C)	time (h)	density (g cm^{-3})	c/a	S_{BET} (m^2 g^{-1})	d_{BET} (nm)	d_{XRD} (nm)	d_{v50} (nm)	span
650	4	5.67 (94%)	1.006	19.1	55	24		
700	2	5.73 (95%)	1.006	17.4	60	32	140	0.9
800	2	5.87 (98%)	1.006	12.6	81	52	143	0.9
800 BTSS[a]	*8*	*5.78 (96%)*	*1.0045*	*9.3*	*112*	*31*	*274*	*1.4*

[a] Reference sample prepared by conventional solid-state reaction from a mechanical mixture of nanocrystalline raw materials.

cubic or pseudocubic structure and low density.[53] This behavior was ascribed to the incorporation of hydroxyl groups into the perovskite lattice. Powders with comparable specific surface area manufactured by companies[54] have density and tetragonality lower than or, at most, comparable to those of the powder described in the present study. The absence of evident internal porosity inside the primary nanocrystals (see Figure 8 and the Supporting Information, Figure S2) strongly indicates that the lower density of the powder in comparison to the theoretical density is likely to be ascribed, at least in part, to the presence of the grain boundaries between the nanograins composing the secondary particles. The product obtained at 800 °C has higher density (98% against 96%) and tetragonality (1.006 against 1.0045) than the reference BTSS powder. The frequency particle size distributions (PSD, volume) of some of the powders reported in Table 1 are shown in Figure 10 and compared to the PSD of the BTSS powder. Powders obtained by the calcination of the $BaCO_3$@TiO_2 particles at 700−800 °C have a median diameter (d_{v50}) of ∼140 nm and a narrow PSD with practically no aggregates bigger than 300 nm. In contrast, the BTSS powders produced by the conventional solid-state process (800 °C) consist of coarser particles (d_{50} = 274 nm) with a broader PSD (aggregates up to 800 nm). Moreover, pure $BaTiO_3$ could not be obtained from BTSS at temperatures lower than 800 °C.

Summary and Conclusions

The formation temperature of $BaTiO_3$ by solid-state reaction between $BaCO_3$ and TiO_2 can be strongly reduced by using $BaCO_3$@TiO_2 core−shell particles as a precursor instead of a mechanical mixture of the raw materials.

Fine $BaCO_3$ acicular crystals have been coated with a layer of amorphous titania by means of a precipitation process. For this purpose, the $BaCO_3$ powder has been suspended in a solution of peroxotitanium(IV) complex. The titanium precursor solution has been prepared from an acidic solution of $TiOCl_2$ by first adding H_2O_2 and then aqueous ammonia until the pH attains a value of 9−10. Formation of the amorphous titania shell on the carbonate crystals is induced by heating the suspension at 90−100 °C. TEM observation has shown the presence of a homogeneous and uniform coating.

Single-phase nanocrystalline barium titanate is obtained by a single-step solid-state reaction of the $BaCO_3$@TiO_2 particles at a temperature of 600−650 °C. This remarkably low temperature makes the solid-state synthesis of nanocrystalline $BaTiO_3$ from core−shell particles competitive with the oxalate route. The lowering of the reaction temperature is around 300−400 °C in comparison to conventional mixtures of micrometer-sized reactants and 150−200 °C in comparison to mechanical mixtures obtained from nanocrystalline raw materials. The final particles have no memory of the initial shape of the $BaCO_3$ crystals because the partially transformed $BaCO_3$@TiO_2 structures undergo a spontaneous fragmentation and spheroidization process during the reaction. Final powders possess high density (94−98% of the theoretical density of macroscopic single crystals), high tetragonality (c/a = 1.006), and a narrow particle size distribution. The median diameter (d_{v50} from volume distribution) is ∼140 nm with a span ($d_{v90} - d_{v10}$)/d_{v50} of 0.9 and no agglomerates bigger than 300 nm.

The solid-state synthesis of nanocrystalline $BaTiO_3$ from $BaCO_3$@TiO_2 particles has unquestionable advantages as compared to the conventional solid-state process. Barium titanate powders obtained by the described process have the potential to be used for the manufacturing of very thin dielectric layers in multilayer ceramic capacitors and other passive components.

As a general conclusion, fine, uniform, and poorly aggregated powders can be obtained by the conventional (and often cheaper) solid-state route using core−shell particles as a precursor, provided mechanisms similar to those previously described are involved. As a further advantage, the formation of a second phase or, more generally, the existence of local chemical fluctuations in the final product, usually arising from poor or incomplete mixing of the raw materials, will be drastically reduced. The size and the morphology of the final product particles can be tailored by varying the size and the shape of the core. Therefore, the core particle acts also as a template and not only as a reactant.

Acknowledgment. Prof. M. Carnasciali, Department of Chemistry and Industrial Chemistry, University of Genoa, is thanked for the Raman measurements. Dr. P. Bowen and Prof. H. Hofmann, Powder Technology Laboratory, EPFL, Lausanne, are gratefully acknowledged for the particle size distribution measurements.

Supporting Information Available: Morphology of the starting $BaCO_3$ crystals (Figure S1), HRTEM image of a $BaTiO_3$ nanocrystal (Figure S2), morphology (SEM) of the final $BaTiO_3$ nanopowder (Figure S3), XRD pattern (Figure S4), and Raman spectrum (Figure S5) of nanocrystalline $BaTiO_3$ (PDF). This material is available free of charge via the Internet at http://pubs.acs.org.

CM061823B

(53) (a) Hennings, D.; Schreinemacher, S. *J. Eur. Ceram. Soc.* **1992**, *9*, 41. (b) Her, Y.-S.; Matijevic, E.; Chon, M. C. *J. Mater. Res.* **1995**, *10*, 3106. (c) Pinceloup, P.; Courtois, C.; Leriche, A.; Thierry, B. *J. Am. Ceram. Soc.* **1999**, *82*, 3049. (d) Hennings, D. F. K.; Metzmacher, C.; Schreinemacher, B. S. *J. Am. Ceram. Soc.* **2001**, *84*, 179. (e) Reveron, H.; Aymonier, C.; Loppinet-Serani, A.; Elissalde, C.; Maglione, M.; Cansell, F. *Nanotechnology* **2005**, *16*, 1137.

(54) Tsurumi, T.; Sekine, T.; Kakemoto, H.; Hoshina, T.; Nam, S.-M.; Yasuno, H.; Wada, S. *J. Am. Ceram. Soc.* **2006**, *89*, 1337.